Atomic-scale visualization and surface electronic structure of the hydrogenated diamond C(100)-(2×1):H surface

Kirill Bobrov,[1] Andrew Mayne,[1] Geneviève Comtet,[1,2] Gérald Dujardin,[1,2] Lucette Hellner,[1,2] and Alon Hoffman[3]
[1]*Laboratoire de Photophysique Moléculaire, Bâtiment 210, Université Paris-Sud, 91405 Orsay Cedex, France*
[2]*Laboratoire pour l'Utilisation du Rayonnement Electromagnétique (LURE), Bâtiment 209D, Université Paris-Sud, 91405 Orsay Cedex, France*
[3]*Department of Chemistry and Solid State Institute, Technion Israel Institute of Technology, Haifa 32000, Israel*
(Received 13 December 2002; revised manuscript received 4 August 2003; published 21 November 2003)

The surface electronic structure of the hydrogenated diamond C(100)-(2×1):H surface was studied using scanning tunneling microscopy (STM), valence band and core-level photoemission, and near-edge x-ray-absorption fine structure. The hydrogenated diamond surface was prepared *ex situ* by hydrogen plasma treatment. The STM topographies of the hydrogenated diamond surface, recorded with an atomic resolution, indicated the atomically smooth diamond surface. The current-voltage (*I-V*) spectroscopy was used to study the transport of electrons injected from the STM tip into the diamond surface. It has been shown that the electron transport is determined not only by the surface states available but it depends crucially on the amount of subsurface hydrogen and the charge redistribution at the surface. Annealing of the diamond surface induces desorption of the subsurface hydrogen. That affects the electron transport as evidenced from the analysis of the *I-V* spectroscopy curves. A qualitative model for the electron transport, taking into account the specific electronic structure of the hydrogenated diamond surface, has been proposed.

DOI: 10.1103/PhysRevB.68.195416 PACS number(s): 73.20.−r, 68.37.Ef, 61.10.Ht

I. INTRODUCTION

In the last ten years the study of hydrogenated and clean diamond surfaces has been a topic of large interest. This is motivated by the fact that hydrogen, chemisorbed on the diamond surface, modifies significantly its surface electronic structure. The hydrogenated diamond surface becomes a *p*-type electrical semiconductor[1–3] whereas the bulk diamond is an almost perfect insulator. The fact that the conductivity is induced by *adsorbed* species provides the unique possibility to control the conductivity *in situ*, at the atomic scale, by manipulation of the individual adsorbed atoms and molecules. Recently, it was demonstrated that a fully hydrogenated diamond surface can be patterned by local removing of hydrogen adatoms using atomic force microscopy (AFM).[4,5] The mechanism of the surface conductivity is, however, not well understood yet. At present there are ongoing debates on the origin and mechanism of the surface conductivity.[6,7] It was demonstrated recently that scanning tunneling microscopy (STM) represents a powerful tool to visualize diamond surfaces (both hydrogenated[8] and clean[9]) at the atomic scale. To use STM to inject electrons and/or holes into a sample seems to be a promising technique to study the surface conductivity of diamond. This is due to the unique feature of the hydrogenated diamond surface: the electron/hole transport occurs mainly through the surface conductive layer.[5]

In this paper we used *I-V* spectroscopy as a tool to study the electron transport through the hydrogenated diamond surface. To quantify changes in the electron transport occurring during thermal annealing, combined surface science techniques [valence band, core-band photoemission, and near-edge, x-ray-absorption fine structure (NEXAFS)] were used to characterize the state of the annealed diamond surface.

II. EXPERIMENT

Semiconducting boron-doped (type IIb) natural single-crystal diamonds of (100) orientation were used. Prior to insertion into an ultrahigh vacuum chamber, the diamond samples were *ex situ* saturated with hydrogen in a microwave (MW) hydrogen plasma at 800 °C for 1 h. The details of the hydrogenation procedure can be found elsewhere.[10] Two diamond samples, hydrogenated under identical conditions, were studied separately using ultrahigh-vacuum (UHV) STM and synchrotron radiation (Super-ACO, Orsay).

The first hydrogenated diamond sample (size $3.5\times2.5\times0.2\ \mathrm{mm}^3$) was installed into the UHV STM chamber having a base pressure below 2×10^{-11} Torr. The edges of the diamond sample were sandwiched between two molybdenum (Mo) plates. After transfer *in vacuo* into the adjoining UHV chamber ($P<1\times10^{-10}$ Torr), the diamond sample was then heated indirectly, by a hot tungsten filament ($t<1400\,°C$) located about 1 cm behind the surface. This preheating procedure was necessary to decrease the sample resistance by thermal activation of dopants. When the resistance of the warm sample had dropped sufficiently, the hot filament was switched off and further annealing was done by applying a bias ($U=70-90$ V, $I=20-60$ mA) directly across the sample. Diamond does not emit light in the infrared region with increased temperature. So the diamond temperature was taken as the temperature of the Mo plate (controlled by an IR pyrometer) in contact with the sample. Initially the diamond sample was annealed at 300 °C for 5 min. All the *I-V* spectroscopy curves were recorded at constant height mode at room temperature. At each temperature the *I-V* curves were then averaged over 400 curves. The originally recorded *I-V* curves were differentiated numerically to calculate the dI/dV spectra.

The second hydrogenated diamond sample (size $6\times1\times0.2\ \mathrm{mm}^3$) was installed into the UHV chamber connected to the synchrotron radiation source. Thermal annealing of the sample was done *in situ* by resistive heating under the same conditions described above. The photoemission spectra as a

function of temperature were always recorded at room temperature when the sample had cooled down after the corresponding annealing. All the photoemission measurements were done at grazing incident angles in order to improve the surface sensitivity. The photoemission spectra were normalized to the photon beam intensity.

Since the diamond temperature was taken as the temperature of the attached Mo plate, we estimate the uncertainty in the diamond temperature to be within ± 50 °C.

The clean diamond surface was prepared *in situ* by resistive heating of the hydrogenated C(100)-(2×1):H sample as described elsewhere.[24] We carefully controlled the cleanness of the diamond surface. No traces of molybdenum were detected at any annealing temperature as evidenced by x-ray photoemission spectroscopy (XPS). The *in situ* hydrogen adsorption on the clean diamond C(100)-(2×1) surface was done as follows. Molecular hydrogen was introduced into the UHV chamber at a pressure of about 10^{-7} Torr. The activation of molecular hydrogen was done using a tungsten filament heated at 1800 °C and located at about 1 cm in front of the sample.

Ultraviolet photoemission spectra were recorded at an incident angle, $\theta_i = 63°$ using 50-eV photons. This photon energy was chosen to obtain the maximum sensitivity to the changes occurring in the photoemission spectra under the annealing. Emitted photoelectrons ($\theta_e = 27°$) were analyzed using a hemispherical electrostatic analyzer with a 250-meV resolution. C($1s$) photoemission spectra were recorded at an incident angle, $\theta_i = 63°$ at two photon energies: 318 and 600 eV. At 318 eV, the kinetic energy of escaping C($1s$) photoelectrons was about 35 eV; this provided the best surface sensitivity.[11] The C($1s$) photoemission spectrum at 600 eV was recorded as a reference in order to estimate the oxygen coverage. The C($1s$) photoemission spectra at both photon energies were corrected by subtraction of the secondary electron background. O($1s$) spectra were recorded at 600 eV; at this energy the best separation between the O($1s$) photoemitted electrons and secondary electron background was achieved.

NEXAFS spectra were recorded in the 280–293-eV photon energy range. Secondary electrons of 35-eV kinetic energy were detected using the electron analyzer. As in the case of the C $1s$ photoemission, the 35-eV kinetic energy gave the highest surface sensitivity. The photon energy was calibrated using the second absolute band gap of diamond at 302.4 eV.[12]

III. RESULTS AND DISCUSSION

A. Atomic scale visualization of the C(100)-(2×1):H surface

The STM topographies of the hydrogenated C(100)-(2×1):H surface, recorded by tunneling through either the unoccupied or the occupied surface states, are shown in Figs. 1(a) and (b), respectively. The bright lines correspond to the CH-CH dimer rows of the (2×1) reconstructed surface. The dimer rows run in orthogonal directions due to the existence of surface domains (terraces) each separated by a step. In Fig. 1(a) we highlighted the C-C dimer rows in vicinity of the S_A monoatomic step. As shown in Fig. 1(b) the distance between the bright lines ($\Delta = 5.0 \pm 0.2$ Å) corresponds well to the expected inter-row distance (5.04 Å) of the (2×1) reconstructed surface. The bright beam-shape features within the bright lines, separated by 2.5 ± 0.2 Å, were ascribed to single CH-CH dimers. Defect structures, such as point defects and missing rows [marked by arrows in Fig. 1(a)], were commonly observed but they are beyond the scope of this study. The I-V spectroscopy curves, reported in this study, were always taken on the flat hydrogenated terraces of the C(100)-(2×1):H surface.

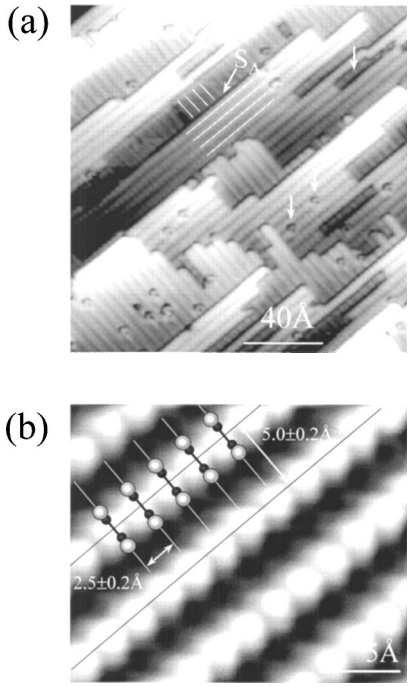

FIG. 1. STM topographies of the hydrogenated diamond C(100)-(2×1):H surface: (a) $U_{\text{bias}} = +1.5$ V, $I_t = 1.5$ nA (unoccupied states), and (b) $U_{\text{bias}} = -1.5$ V, $I_t = 1.0$ nA (occupied states). The bright lines on the top topography indicate the C-C dimer rows in the vicinity of the step (S_A).

B. Unoccupied states of the hydrogenated C(100)-(2×1):H surface

First, we consider the I-V spectroscopy curve, recorded just after the initial thermal annealing at 300 °C. For the outgazed surface, a very steep current increase was observed at positive bias [Fig. 2(a)]. We were able to measure the current only up to $U_{\text{bias}} = +0.6$ V, at higher biases the current exceeded the 50-nA saturation limit of the current amplifier. The fact that a large tunneling current can be reproducibly obtained at positive bias would suggest the existence of unoccupied states above the Fermi level in the fundamental band gap. However, density-of-states (DOS) calculations[13,14] as well as the photoabsorption experiments[15] show that no unoccupied states exist on the hydrogenated diamond surface in the 0–+3-eV binding-energy range. The MW-hydrogenated surface used in this study does not represent, however, a perfect hydrogenated surface. The surface, being well ordered at the atomic scale (Fig. 1), is imperfect in the

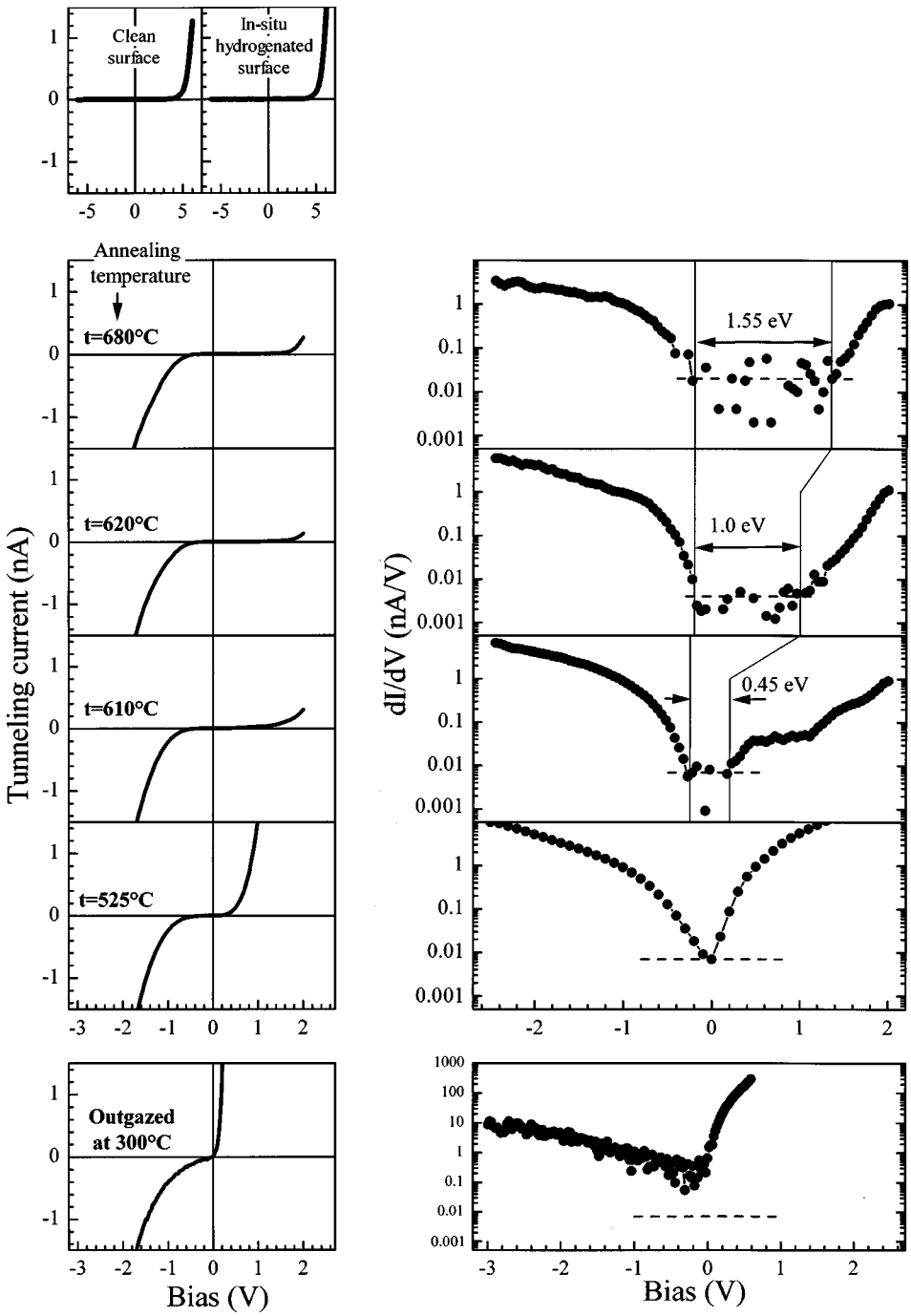

FIG. 2. Current-voltage (I-V) spectroscopy of the hydrogenated C(100)-(2×1):H surface. The I-V spectroscopy curves, as a function of annealing temperature, are shown in the left panel whereas the right panel represents the corresponding dI/dV curves. The vertical solid lines indicate the surface band gap. For each dI/dV curve the dashed lines indicates the detection limit.

sense that during hydrogenation, hydrogen not only saturates the surface dangling bonds[16] but penetrates into the subsurface region.[17,18] The subsurface hydrogen represents surface traps for valence-band electrons. The electron trapping induces hole accumulation in the subsurface region. This charge redistribution can be treated as surface band bending extending several nanometers deep into the bulk diamond (Fig. 3). The significant band bending (see Appendix A) induces partial ionization of the valence-band (VB) states that appear as empty states just above the Fermi level as schematically shown in Fig. 3. These empty states are responsible for the steep current increase at small positive bias observed on the I-V spectroscopy curve shown in Fig. 2(a). The origin of the electron traps, inducing the observed band bending, is probably single dangling bonds produced in the subsurface region by a rupture of C-C bonds in the vicinity of the subsurface hydrogen.[19–23] These dangling bonds are supposed to have a great affinity to electrons due to their unsaturated character.

C. Electron transport in the tip-sample junction as a function of thermal annealing

The I-V spectroscopy curves were recorded as a function of temperature annealing in the 300–680 °C range (Fig. 2). Individual spectroscopy curves were taken on the flat ter-

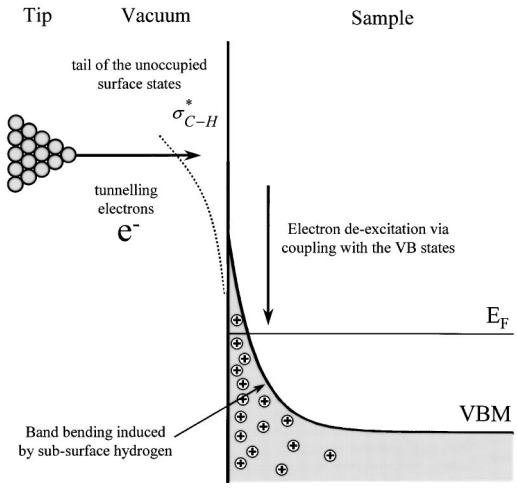

FIG. 3. Schematics of the electron transfer in the tunneling junction between the metallic tip and the hydrogenated diamond surface.

races before averaging together. This meant that surface defects could be avoided. The set point was the same for all the spectroscopy curves: $U_{\text{bias}}=-1.5$ V and $I_t=1.0$ nA. So, the negative part of the *I-V* spectroscopy curves was almost the same independent of the annealing temperature. However, significant changes were observed at positive bias. Mild annealing at $t=525\,^{\circ}$C decreased dramatically the tunneling current. The *I-V* spectroscopy curve could be recorded up to +2.0 V without amplifier saturation. Subsequently we chose to limit the maximum positive bias to +2.0 V for recording *I-V* spectroscopy. At higher biases tip-induced modification of the surface was occasionally observed that affected the *I-V* spectroscopy measurements. Further annealing in the 525–680 °C range induces further decrease of the tunneling current as evidenced by the corresponding *I-V* spectroscopy curves (Fig. 2). To analyze quantitatively these changes a numerical derivation of the *I-V* spectroscopy curves was made (right panel in Fig. 2). For each dI/dV spectrum shown in Fig. 2 we calculated the detection limit (horizontal dashed lines) which was defined here as a threshold at which fluctuations of the dI/dV values due to the thermal noise were observed. We define therefore the surface band gap (marked by thin vertical lines in Fig. 2) as the bias range at which the dI/dV values exceed the detection limit. The existence of a band gap does not mean, of course, the absolute absence of tunnel current in the energy range corresponding to the gap. In fact, we were able to tunnel into unoccupied states at any positive bias. The existence of a band gap simply means that in a certain energy range (and for a given preset tunneling current) the amount of tunnel current was below the detection limit. Accepting this definition, it can be seen in Fig. 2 that the diamond surface after outgassing at ~300 °C demonstrates no surface gap, a gap conductivity being measurable over the whole applied bias range. After annealing at 525 °C the dI/dV values still exceed the detection limit although at $U_{\text{bias}}=0$ they become comparable with it. So the existence of a small gap of ~0.1 eV cannot be excluded in this case. Further annealing at 610 °C increases the surface band gap up to ~0.45 eV (Fig. 2). During the annealing between 620 and 680 °C the surface band gap continues to increase and reaches ~1.55 eV at 680 °C (Fig. 2).

As evidenced in Fig. 2, after the 680 °C annealing there are still states with an energy higher than +1.5 V. These states are obviously too high in energy to be due to band bending. Instead, we believe they are associated with the tails of the unoccupied hydrogen induced surface states as schematically shown in Fig. 3. The exact binding energy of these states is unknown although they definitely exist in the fundamental band gap as evidenced from our earlier NEXAFS studies.[24] These states exist as long as the surface is terminated by hydrogen. They remain unchanged in the 610–680 °C range since the temperature is too low to induce desorption of surface hydrogen.[10]

When the bias is sufficiently high ($U_{\text{bias}}>+1.5$ V) electrons tunnel into the $\sigma^*_{\text{C-H}}$ surface states. These unoccupied states are well localized on the corresponding C-H bonds based on the theoretical analysis of the surface band structure.[13] The localized nature of the $\sigma^*_{\text{C-H}}$ orbitals eliminates any *direct* propagation of electrons through these states. The existence of a tunneling current in a steady-state regime implies that another transport channel exists for the electrons. This channel includes the de-excitation of the electrons temporarily occupying the $\sigma^*_{\text{C-H}}$ states via coupling with those valence-band (VB) states which are shifted above the Fermi level due to the band-bending effects (Fig. 3).

The electron transport through the tunneling junction depends therefore on: (i) the probability of an electron to tunnel through the vacuum gap, (ii) the degree of coupling of the unoccupied surface states with the empty VB states and (iii) the rate of electron/hole recombination in the surface layer. Since the hydrogen termination of the diamond surface is preserved in the 300–680 °C range, no changes are expected in the density of unoccupied surface states. It implies that the probability for electrons to tunnel through the vacuum gap varies very little in this particular case. Thus we can rule out factor (i) as a reason of the observed changes in the *I-V* spectroscopy curves (Fig. 2).

D. Thermally induced processes on the hydrogenated diamond surface

In a separate experiment, we probed the *structure* of the hydrogenated diamond C(100)-(2×1):H surface as a function of thermal annealing. For that purpose, valence-and core-band photoemission spectra as well as NEXAFS spectra were recorded. The diamond sample was annealed at the same temperatures as in the STM experiments. The method for assigning the UPS, XPS, and NEXAFS spectra is given in Appendix B. First we characterized the diamond surface outgassed at 300 °C by VB photoemission. Figure 4 represents the VB photoemission spectra of the ''as hydrogenated'' and the 300 °C annealed surface. The difference between the two spectra is obvious. The S_{Ox} band, induced by water adsorption on the as-hydrogenated surface, disappears after the 300 °C annealing. Further annealing had little influence on the VB photoemission spectra, so the state of the diamond surface was monitored by x-ray photoemission. The C 1*s* photoemission spectra were recorded as a function of

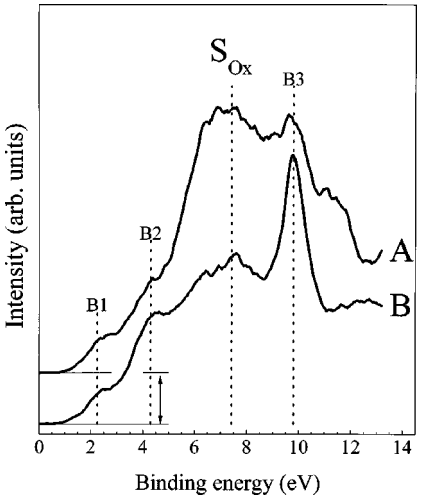

FIG. 4. Valence-band photoemission spectra of the hydrogenated C(100)-(2×1):H surface. Curves A and B correspond to the "as-installed" and outgazed (~300 °C) surfaces, respectively. For clarity, curve A was shifted up as indicated by the arrows.

annealing temperature (Fig. 5, left panel). As evidenced in Fig. 5, annealing at 525 °C induces no changes in the C 1*s* photoemission spectra. Both the binding energies and the integral areas of the bulk and CH_x components were essentially the same before and after the annealing. However, the intensity of the O 1*s* peak decreases after the 525 °C annealing (Fig. 5, right panel). The valence-band photoemission spectra shown in Fig. 4 indicate that water has been desorbed during the 300 °C outgassing. Thus the oxygen contaminants desorbing in this temperature range must be associated with traces of chemisorbed oxygen on the hydrogenated surface.

Considering now the corresponding changes in the *I-V* spectroscopy curve after 525 °C annealing (Fig. 2), one can infer that the surface state coupling with the VB states is very sensitive to the presence of oxygen on the surface. The chemisorbed oxygen on the diamond surface serves as a sink for electrons (in addition to the subsurface hydrogen discussed in Sec. III B). Similar effects associated with water layer adsorption on the hydrogenated diamond surface were recently observed by Mayer *et al.*[25] Thus more holes are produced within the surface layer when chemisorbed oxygen is present on the surface. The VB states penetrate more into the band gap and the surface states are coupled more tightly to the VB states (Fig. 3). Consequently, the partial reduction of this coupling under oxygen desorption at 525 °C is reflected in the *I-V* spectroscopy curve by a significant decrease of the tunneling current at positive bias (Fig. 2).

Further annealing of the hydrogenated diamond surface changes the situation qualitatively. In this temperature range (610 °C) the subsurface hydrogen, which had been incorporated during the surface preparation, effuses out of the sample. The disappearance of the subsurface hydrogen is clearly seen in the core-level photoemission spectra: the C 1*s* (CH_x) component decreases in intensity (Fig. 5, left panel). Only a small fraction of the subsurface hydrogen remains on the surface after the 680 °C annealing (Fig. 5). This is consistent with the maximum hydrogen effusion rate occurring at 720 °C (Ref. 26). The effect of the subsurface hydrogen desorption on the surface electronic structure is twofold. First, the hydrogen effusion reduces by itself the amount of electron traps within the surface layer. As a result, the number of holes decreases and the hole recombination with incoming electrons (injected from the tip) is reduced. Second, the band bending in the surface layer is reduced following the hole reduction. So, the coupling of the surface states with the empty VB states is further reduced. These two effects together induce further current decrease giving rise to a surface band gap (Fig. 2) as was discussed in the previous section. It is interesting to note that only subsurface hydrogen desorbs in this temperature range. The NEXAFS spectra (Fig. 6) indicate that the surface hydrogen remains throughout the thermal treatment: the $Ex_{C\text{-}H}$ resonance (see Appendix B) is still visible in the spectra. The changes in the shape

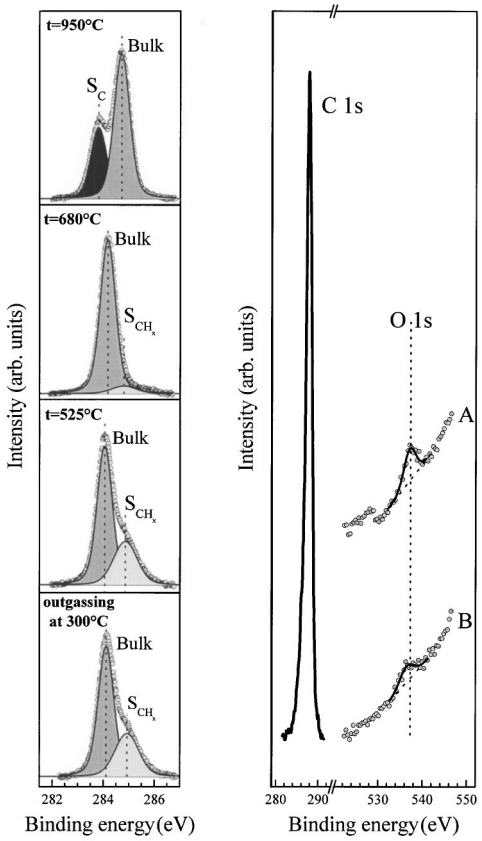

FIG. 5. On the left: C 1*s* photoemission spectra ($h\nu = 318$ eV) recorded as a function of annealing temperature. The circles represent the original data (corrected by background subtraction). The dark-gray (bulk) area represents the bulk C 1*s* component. The light-gray ($S_{C\text{-}H}$) and black (S_C) areas represent the surface C 1*s* components associated with the CH_x species/subsurface hydrogen and dangling bonds of the C-C dimers, respectively. On the right: O 1*s* spectra ($h\nu = 600$ eV) before thermal annealing (curve A) and after (curve B) the $T = 525$ °C annealing. The open circles represent the original data, the dotted lines indicates the background of secondary electrons, and the solid lines represent the fit of the O 1*s* photoemission peak. The C 1*s* photoemission spectrum was recorded at the same photon energy ($h\nu = 600$ eV) to estimate the oxygen coverage on the diamond surface.

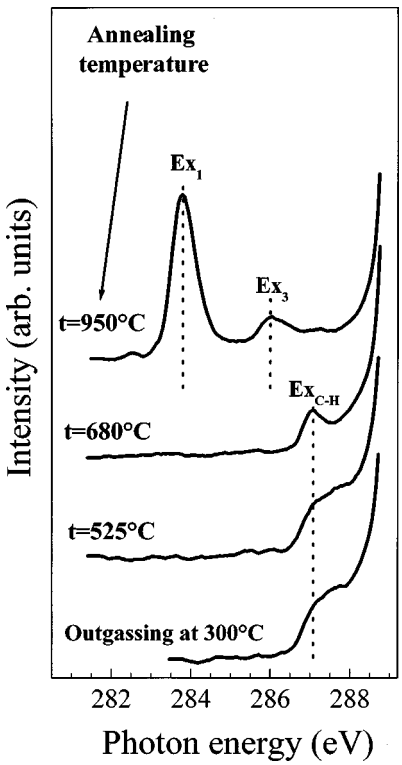

FIG. 6. NEXAFS spectra of the hydrogenated diamond C(100)-(2×1):H surface recorded as a function of annealing temperature.

of the $Ex_{\text{C-H}}$ resonance after the 680 °C annealing are therefore associated with the subsurface hydrogen desorption.

Annealing the hydrogenated diamond surface at higher temperatures ($t = 950\,^{\circ}\text{C}$) induces total desorption of hydrogen, both sub-surface and surface ones, revealing the clean diamond surface. The bulk C($1s$) component is shifted towards higher binding energies, the CH_x component disappears completely and a new S_C component appears in the spectrum (Fig. 5). The NEXAFS spectrum has been changed as well (Fig. 6). The $Ex_{\text{C-H}}$ shoulder disappears whereas the Ex_1 and Ex_3 peaks appear in the spectrum (the notation for the absorption resonances is taken from Ref. 16). Both the C($1s$) (Fig. 5) and NEXAFS (Fig. 6) spectra are characteristic of the clean surface.[24] When using the STM, no tunneling current could be obtained at negative bias.[8] However, electrons could be injected into the conduction band of diamond (if the positive bias is higher than the band gap of diamond, 5.5 eV) and a stable current could be obtained.[8] The I-V spectroscopy curve recorded under such a condition ($U_{\text{bias}} = 5.9$ V, $I_t = 1.0$ nA) is shown in Fig. 2. In order to further elucidate the role of the subsurface hydrogen in the electron transport throughout the diamond surface we have adsorbed *in situ* hydrogen on the clean diamond surface. Interestingly, the *in situ* hydrogenated surface shows exactly the same I-V spectroscopy curve as the clean surface (see Fig. 2). This can be understood by considering that during the *in situ* hydrogenation, hydrogen is adsorbed only saturating the top layer of carbon dangling bonds and that no hydrogen is adsorbed in the subsurface region contrary to the case of the *ex situ* microwave hydrogenation.

IV. CONCLUSION

The surface electronic structure of the hydrogenated diamond C(100)-(2×1):H surface has been studied using both local probe (STM) and other surface science techniques (valence band and core-level photoemission and NEXAFS).

A qualitative model for the electron transport through the metallic tip/hydrogenated diamond surface tunneling junction has been proposed. The electron transport includes the following steps: (i) electron tunneling into the surface states located in the fundamental band gap of diamond, (ii) electronic de-excitation through the surface state coupling with the VB states, and (iii) electron/hole recombination. The electrons, initially emitted from the Fermi level of the tip, tunnel into the tails of the unoccupied surface states associated with the antibonding $\sigma^*_{\text{C-H}}$ orbitals. These electrons gradually lose their energy (de-excitation) through the surface-state coupling with the VB states. The coupling is greatly facilitated due to the upward surface band bending existing on the hydrogenated diamond surface. After the de-excitation process, the injected electrons recombine with the holes initially presented into the subsurface layer. Two factors—the presence of the subsurface hydrogen and traces of chemisorbed oxygen—were found to induce the upward band bending on the hydrogenated diamond surface.

The I-V spectroscopy allowed us to probe the rate-limiting step of the electron transport, namely the surface-state coupling with the VB states and the electron/hole recombination. Thermal annealing of the hydrogenated diamond surface affects significantly the electron transport. Initially, the typical I-V spectroscopy curve demonstrates no surface gap and a strong rectification at positive bias. Annealing at 525 °C removes partially the traces of chemisorbed oxygen without affecting the subsurface hydrogen. This directly influences the electron transport in the tip-sample tunneling junction. The partial reduction in the band bending is reflected in the corresponding I-V curves as a sharp current decrease at positive bias.

Annealing the surface at $T > 610\,^{\circ}\text{C}$ induces gradual desorption of the subsurface hydrogen. Surface band bending is further reduced, leading to a decoupling of the VB and hydrogen induced surface states. The amount of holes in the subsurface layer also decreases as the amount of subsurface hydrogen decreases. As a result, the electron transport is further affected and a surface gap appears in the I-V spectroscopy curves. The surface gap increases from 0.45 eV at 610 °C up to 1.55 eV at 680 °C.

High-temperature annealing at 950 °C induces desorption of the surface hydrogen and reveals the insulating clean diamond surface. Neither surface visualization nor probing surface electronic structure was possible under normal tunnel conditions.

ACKNOWLEDGMENTS

We wish to thank the European IST-FET ''Bottom-up-Nanomachines'' (BUN) and the European ''Atomic and Molecular Manipulation: A new tool In Science and Technology'' (AMMIST) network.

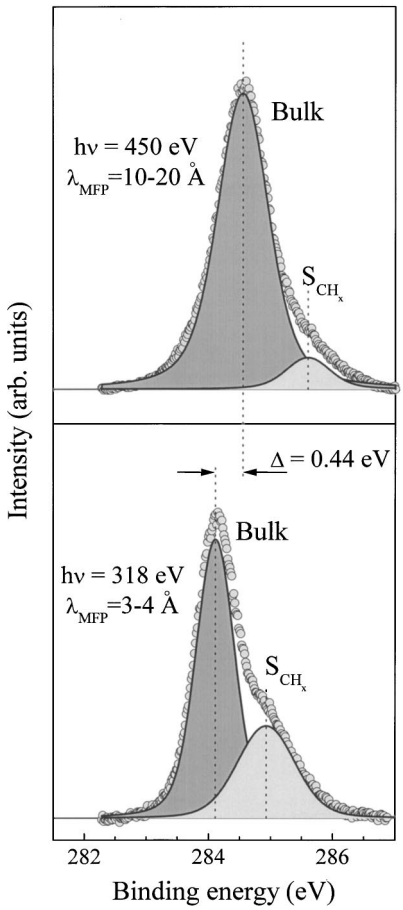

FIG. 7. C 1*s* photoemission spectra recorded on the 300 °C annealed surface at photon energies of 450 and 318 eV. The circles represent the original data. The dark-gray area represents the bulk C 1*s* component and the light-gray areas represent the C 1*s* component corresponding to the subsurface hydrogen. The energy shift of the bulk C 1*s* component is marked by arrows. The mean free path (λ_{MFP}) of electrons is indicated.

APPENDIX A: QUANTITATIVE ANALYSIS OF THE BAND BENDING ON THE C(100)-(2×1):H SURFACE

To evaluate the surface band bending we recorded photoemission spectra using the synchrotron radiation source (see Sec. II). The spectra, recorded at 450- and 318-eV photon energies, are shown in Fig. 7. These photon energies were chosen to give photoemitted electrons with kinetic energies of 165 and 33 eV, with respect to the binding energy of the bulk C(1*s*) component at 285.0 eV.[27] The 33-eV kinetic energy electrons have the shortest mean free path of 3–4 Å while a longer mean free path of 10–20 Å is expected for the 165-eV kinetic energy electrons.[28] This difference means that by varying the photon energy we can probe C(1*s*) electrons escaping from different depths below the diamond surface. It can be seen in Fig. 7 that the binding energy of the electrons (284.11 eV) escaping from the 3–4-Å depth is 0.44 eV lower than that of electrons escaping from the 10–20-Å depth (284.55 eV). It directly implies that upward band bending exists on the hydrogenated diamond surface.

APPENDIX B: ASSIGNMENT OF THE PHOTOEMISSION AND PHOTOABSORPTION SPECTRA

The photoemission bands of Fig. 4—B_1, B_2, B_3, S_{Ox}—were assigned as follows. The B_1, B_2, B_3 bands were assigned to the bulk diamond because: (i) their appearance does not depend on the state of the diamond surface,[29] and (ii) all these bands are strongly dispersed with the photon energy, which is characteristic of bulk diamond transitions.[29] The S_{Ox} band, centered at 7.4 eV, was assigned to the oxygen contaminants adsorbed on the hydrogenated diamond surface under its exposure to ambient air.[25] The binding energy of this band (7.4 eV) differs significantly from that of chemisorbed oxygen (~3 eV) on the diamond surface,[30] so this band was assigned to the photoemission from the nonbonding orbitals of adsorbed water. The same photoemission band was observed after water adsorption on the Si(100) surface.[31]

The x-ray photoemission spectra of Figs. 5 and 7 were deconvoluted to resolve the C(1*s*) components. The details of the deconvolution procedure can be found elsewhere.[24] The assignment of the C(1*s*) components was done as follows. The bulk component was assigned to the bulk diamond and/or C-H monohydride on the diamond surface. These two components have the same binding energy and, consequently, are indistinguishable in the C(1*s*) spectra.[24] The S_C component was observed on the clean diamond surface only and has been previously assigned to the surface carbon dimers.[24] The S_{CH_x} component was detected previously on the *ex situ* prepared diamond surface only (absent on the *in situ* prepared hydrogenated surface) and was assigned to the nonmonohydride CH_x species.[24] Here, we can further elaborate its origin. Taking into account that the atomically smooth diamond surface (Fig. 1) can be produced by the hydrogenation procedure, we conclude that this peak mainly originates from the subsurface hydrogen. This conclusion is supported by the fact that the binding energy of the C(1*s*) (CH_x) component depends on the depth from which the photoemitted electrons escape (Fig. 7). The C(1*s*) (CH_x) component originating from the 3–4-Å depth has a lower binding energy than the one corresponding to the 10–20-Å escaping depth (Fig. 7). This observation illustrates once again the band bending in the surface layer (see Appendix A) and directly suggests that the C(1*s*) (CH_x) component originates from the species distributed in the surface layer, i.e., subsurface hydrogen.

The assignment of the photoabsorption peaks in the NEXAFS spectra was done as follows. The $Ex_{C\text{-}H}$ resonance located at 287.1 eV was interpreted as an electron transition from the C(1*s*) level to the unoccupied σ^* antibonding state of the C-H monohydride according to Hoffman *et al.*[12] The Ex_1 and Ex_3 resonances, located at 283.8 and 286.0 eV, respectively, have been previously assigned to the surface core resonances associated to π-bonded dangling bonds of the C-C dimers on the clean diamond C(100)-(2×1) surface.[32]

[1] H. J. Looi, L. Y. S. Pang, A. B. Molloy, F. Jones, J. S. Foord, R. B. Jackman, Diamond Relat. Mater. **7**, 550 (1998).
[2] H. J. Looi, M. D. Whitfield, J. S. Foord, and R. J. Jackman, Thin Solid Films **343–344**, 623 (1999).
[3] O. A. Williams, M. D. Whitfield, R. B. Jackman, J. S. Foord, J. E. Butler, and C. E. Nebel, Diamond Relat. Mater. **10**, 423 (2001); Appl. Phys. Lett. **78**, 3460 (2001).
[4] M. Tachiki, T. Fukuda, K. Sugata, H. Seo, H. Umezawa, and H. Kawarada, Jpn. J. Appl. Phys., Part 1 **39**, 4631 (2000).
[5] M. Tachiki, T. Fukuda, K. Sugata, H. Seo, H. Umezawa, and H. Kawarada, Appl. Surf. Sci. **159–160**, 578 (2000).
[6] B. Koslowski, S. Strobel, and P. Zeiman, Phys. Rev. Lett. **87**, 209705 (2001).
[7] F. Maier, M. Riedel, B. Mantel, J. Ristein, and L. Ley, Phys. Rev. Lett. **87**, 209706 (2001).
[8] R. E. Stallcup II and J. M. Perez, Phys. Rev. Lett. **86**, 3368 (2001).
[9] K. Bobrov, A. Mayne, and G. Dujardin, Nature (London) **413**, 616 (2001).
[10] K. Bobrov, H. Shechter, M. Folman, and A. Hoffman, Diamond Relat. Mater. **7**, 170 (1998).
[11] J. F. Morar, F. J. Himpsel, G. Hollinger, J. L. Jordon, G. Hughes, and F. R. McFeely, Phys. Rev. B **33**, 1346 (1986).
[12] A. Hoffman, G. Comtet, L. Hellner, G. Dujardin, and M. Petravic, Appl. Phys. Lett. **73**, 1152 (1998).
[13] J. Furtmuller, J. Hafner, and G. Kresse, Phys. Rev. B **53**, 7334 (1996).
[14] G. Kern, J. Hafner, and G. Kresse, Surf. Sci. **352–354**, 745 (1996).
[15] E. Rohrer, C. F. O. Graeff, R. Janssen, C. E. Nebel, and M. Stutzmann, Phys. Rev. B **54**, 7874 (1996).
[16] R. Graupner, M. Hollering, A. Ziegler, J. Ristein, and L. Ley, Phys. Rev. B **55**, 10 841 (1997).
[17] A. Laikhtman, A. Hoffman, and C. Cytermann, Appl. Phys. Lett. **79**, 1115 (2001).
[18] J. Chevallier, B. Theys, A. Lusson, C. Grattepain, A. Deneuville, and E. Gheeraert, Phys. Rev. B **58**, 7966 (1998).
[19] J. P. Goss, R. Jones, M. I. Heggie, C. P. Ewels, P. R. Briddon, and S. Öberg, Phys. Rev. B **65**, 115207 (2002).
[20] D. F. Talbot-Ponsonby, M. E. Newton, J. M. Baker, G. A. Scarsbrook, R. S. Sussmann, A. J. Whitehead, and S. Pfenninger, Phys. Rev. B **57**, 2264 (1988); X. Zhou, G. D. Watkins, K. M. McNamara Rutledge, R. P. Messmer, and Sanjay Chawla, *ibid.* **54**, 7881 (1996).
[21] H. J. Looi, L. Y. S. Pang, M. D. Whitfield, J. S. Foord, and R. B. Jackman, Diamond Relat. Mater. **9**, 975 (2000).
[22] D. Takeuchi, S. Yamanaka, and H. Okushi, Diamond Relat. Mater. **11**, 355 (2002).
[23] C. Sauerer, F. Ertl, C. E. Nebel, M. Stutzmann, P. Bergonzo, O. A. Williams, and R. A. Jackman, Phys. Status Solidi A **186**, 241 (2001).
[24] K. Bobrov, G. Comtet, G. Dujardin, L. Hellner, Ph. Bergonzo, and C. Mer, Phys. Rev. B **63**, 165421 (2001).
[25] F. Maier, M. Riedel, B. Mantel, J. Ristein, and L. Ley, Phys. Rev. Lett. **85**, 3472 (2000).
[26] M. C. Rossi, S. Salvatori, F. Scotti, G. Conte, and E. Cappelli, Phys. Status Solidi A **181**, 29 (2000).
[27] J. F. Morar, F. J. Himpsel, G. Hollinger, J. L. Jordan, G. Hughes, and F. R. McFeely, Phys. Rev. B **33**, 1340 (1986).
[28] B. B. Pate, Surf. Sci. **165**, 83 (1986).
[29] K. Bobrov, G. Comtet, G. Dujardin, and L. Hellner, Surf. Sci. **482–485**, 437 (2001).
[30] J. C. Zheng, X. N. Xie, A. T. S. Wee, and K. P. Loh, Diamond Relat. Mater. **10**, 500 (2001).
[31] R. K. Shulze and J. F. Evans, Appl. Surf. Sci. **81**, 449 (1994).
[32] R. Graupner, J. Ristein, L. Ley, and Ch. Jung, Phys. Rev. B **60**, 17 023 (1999).